



Effect of the surface roughness on the measured thermal diffusivity of the ZnBeMnSe single-crystalline solids

K. Strzałkowski¹ · M. Pawlak¹ · S. Kulesza² · D. Dadarlat³ · M. Streza³

Received: 27 March 2019 / Accepted: 6 June 2019 / Published online: 12 June 2019
© The Author(s) 2019

Abstract

In this work, the influence of the surface treatment of bulk samples of the single-crystals observed by means of the Atomic Force Microscopy on the measured thermal diffusivity of the material is presented and discussed. The mixed $Zn_{1-x-y}Be_xMn_ySe$ crystals were grown from the melt by the modified high-pressure Bridgman method with different Be and Mn contents. The investigated specimens were first ground, then polished, chemically etched and finally annealed in zinc vapor. After each surface technological preparation the AFM images were taken and the thermal diffusivity of $Zn_{1-x-y}Be_xMn_ySe$ compounds was determined by the photopyroelectric technique in the back configuration. The ground sample exhibited the highest roughness, whereas the annealed sample showed the lowest one. It has also been shown that the thermal diffusivity of the ground sample was significantly lower compared to the samples whose surface has been treated by other procedures. It was assumed that the measured thermal diffusivity had an effective value attained through the mediation of the thermal parameters of the bulk sample with those of the damaged surface layer. To analyze the results, a two-layer model proposed by J.J. Alvarado-Gil was employed. It turned out that the effective thermal diffusivity value depends much stronger on the conductivity of the system than on the diffusivity of the bulk.

1 Introduction

The paper presents the results concerning the influence of different surface treatments (grounding, polishing, etching and annealing) of the quaternary semiconductor mixed crystals over the thermal diffusivity measurements. The thermal diffusivity is a bulk property of a material, related to the speed of the thermal wave to reach the thermal equilibrium, under variable thermal conditions. The thermal diffusivity can be measured with other various techniques [1, 2], but in this work the photopyroelectric method in the back detection configuration (BPPE) was applied [3, 4]. After each step

of the technological treatment, the surface of the selected crystal was investigated with AFM technique. Since PPE is a contact investigation method, one can expect to find a difference between the surface treatment procedures and the measured thermal diffusivity of the investigated samples. On the other hand, the treatment procedure could influence not only the quality of the contact surface, but also the quality of the whole crystal, which could lead to different heat transfer through the material and hence to different values of the thermal parameters. A proper surface preparation is important not only in the case of bulk samples but especially for thin layer systems, where the roughness of the surface can play much more important role. Therefore, this study is also important in terms of applied physics.

The PPE technique in a first approximation assumes a perfect thermal contact between the sample and the sensor. This assumption is valid only for liquid samples. In reality, a solid sample will always exhibit some surface imperfections. Even more, one needs some fluid (called coupling fluid) to glue somehow the sample to the sensor. It has also already been shown by several researchers how the presence of a coupling fluid can influence the results obtained with PPE technique [5–8]. It was demonstrated that even 1 μm layer of a coupling liquid can change the slope of the phase-root

✉ K. Strzałkowski
skaroll@fizyka.umk.pl

¹ Institute of Physics, Faculty of Physics, Astronomy and Informatics, Nicolaus Copernicus University, Grudziadzka 5, 87-100 Torun, Poland

² Faculty of Mathematics and Computer Science, Warmia and Mazury University in Olsztyn, Słoneczna 54, 10-710 Olsztyn, Poland

³ National R&D Institute for Isotopic and Molecular Technologies, Donat Str. 67-103, POB-700, 400293 Cluj-Napoca, Romania

frequency graph, especially in case of highly conductive or thin samples [5, 8]. It was also shown that thanks to some optimization procedures, this drawback could be minimized [8].

The surface roughness problem was also considered in the case of PTR (photothermal radiometry) technique [9–17]. In the PTR technique one heats up the surface of the sample and measures the thermal radiation using an infrared sensitive device [18]. Since the signal in this technique is collected directly from the surface, the proper treatment of the surface of the sample is of high importance in the case of the infrared opaque samples. On the other hand, for non-infrared opaque sample the ideal preparation of the surface is not necessary [19]. The generation of the PTR signal in the case of the rough surface was often modeled by an equivalent layer model, assuming a plane sample with a surface layer having both effective thermal properties and a thickness dependent on the roughness parameter [11]. Some authors have interpreted the responses of the rough surface by assuming a decrease of the thermal effusivity of the subsurface [12] or/and a shortening of the thermal diffusion length [13]. Walter et al. [14] proposed to consider an equivalent coating layer by interpreting the cross-section of a rough sample as an equivalent thermal circuit consisting of the thermal resistors connected in parallel. Walter made numerous improvements later using fractal analysis [10]. The influence of the roughness was also modeled by representing its effect as random noise having a Gaussian distribution [15, 16]. On the other hand Antoniov et al. [9] proposed a simpler approach by modifying the effective surface layer model by including effective optical absorption and reflection coefficients linked to the state of the surface. They have demonstrated that this assumption could be used on a wide range of the roughness of the surface of the sample. The surface roughness was also considered as important parameters affecting the photothermal imaging [17]. To reduce the signal noise in the case of the imaging some comprehensive criteria were proposed. In summary, many authors were dealing with the roughness of the surface of the sample being investigated, but none in the case of PPE technique. To our best knowledge, there is no papers dealing with the influence of the roughness of the sample in case of the photopyroelectric calorimetry method. We will show that appropriate preparation of the samples is necessary to get the right thermal parameter values in both, contact and non-contact techniques.

2 Materials and methods

The crystals under investigation were grown from the melt using high purity powders of ZnSe, Be, Mn and Se with modified Bridgman-Stockbarger method [20]. The crystal rods were cut perpendicular to the growth axis into about

1.5 mm thick wafers. The samples were first ground by using grinding powder (Al_2O_3 , 10 μm in diameter), next polished with diamond paste (1 μm) and finally chemically etched in a solution of sulfuric acid (96%), potassium dichromate and water. After the polishing procedure, the selected samples were additionally annealed in zinc vapor at 1300 K for 48 h. After each step of surface treatment, photopyroelectric and AFM studies have been performed.

The real composition of the investigated crystals was measured with the scanning electron microscopy/energy dispersive spectroscopy (SEM/EDS) analysis. Measurements were performed with scanning transmission microscope SEM-LEO 1430VP, made by LEO Electron Microscopy Ltd, Cambridge, England and x-ray spectrometer (energy-dispersive mode) Quantax 200, made by Bruker-AXS Microanalysis GmbH, Berlin, Germany, with EDX XFlash 4010 detector. The results showed that the investigated samples were spatially uniform in composition. The Be content was calculated assuming that the sum of cations content in at. % (Zn, Mn, Be) is equal to that of Se anion [21]. The structure of the measured crystalline alloys was determined with x-ray diffraction method, which confirmed that the samples exhibited a sphalerite structure, typical for pure ZnSe crystal [22]. Both $\text{Zn}_{1-x}\text{Mn}_x\text{Se}$ [23] and $\text{Zn}_{1-x}\text{Be}_x\text{Se}$ [22] ternary alloys exhibit sphalerite structure as the content of the beryllium and manganese do not exceed 0.2. Because this is the case of our mixed $\text{Zn}_{1-x-y}\text{Be}_x\text{Mn}_y\text{Se}$ crystals, a zinc blende structure was expected.

The experimental setup for the PPE measurements [8] consisted of a blue diode laser (405 nm) with the output power of about 300 mW, a LiTaO_3 detector (0.4 mm thickness) with Cr + Au electrodes and a SR850 lock-in for processing the measured signal. The laser spot was set to about 3 mm in diameter to satisfy the 1D-heat propagation assumption through the sample. A thin layer of ethylene glycol served as a coupling fluid between the sample and the sensor. The detector was protected from accidental illumination by a black diaphragm. Frequency scans were performed in the 1–15 Hz range, with 0.5 Hz single step.

The AFM measurements were carried out using Multi-mode eight (Bruker) instrument working in an MFM (Magnetic Force Microscopy) mode. Imaging of magnetic domains makes use of the ferromagnetic tapping probe (MESP by Bruker) to scan the surface topography at a low tip-surface distance and following the same track at increased lift to detect magnetic interactions. The MESP probe characteristics are tip radius 20 nm, resonant frequency 75 kHz, spring constant 2.8 N/m, magnetic coating (10–150 nm of Co/Cr), coercivity 400 Oe. A lateral resolution of the sample topography is limited by the tip radius, but on the other hand, the MFM resolution is roughly equal to the lift height (not less than 20–50 nm), although additional van der Waals forces might influence the tip-surface interactions at very low lift values.

The measurements were performed at room temperature and ambient conditions.

3 Theory

In a back PPE four-layer system an optically opaque sample s is placed on a pyroelectric sensor p and the whole system remains surrounded by the air (front and back layers, see Fig. 1).

Assuming a perfect sample-sensor thermal contact and a one-dimensional model of the heat propagation through the sandwich-like multi-layered system, the complex PPE signal is given by the following formula [3, 24, 25]:

$$V = \frac{2V_0 e^{-\sigma_s L_s}}{b_{sp} + 1} \frac{1 - e^{-2\sigma_p L_p}}{1 + R_{sp} e^{-2\sigma_p L_p} - (R_{sp} + e^{-2\sigma_p L_p}) e^{-2\sigma_s L_s}} \quad (1)$$

where V_0 is an instrumental factor, ij represents s and p layers of the detection cell, respectively, $R_{ij} = (b_{ij} - 1)/(b_{ij} + 1)$ is the reflection coefficient of the thermal wave at ij interface, $b_{ij} = e_i/e_j$ where e is thermal effusivity, $\sigma_i = (1 + i)a_i$ is the complex diffusion coefficient, a_i is the reciprocal of the thermal diffusion length μ_i , $a_i = 1/\mu_i$, $\mu_i = (2\alpha_i/\omega)^{1/2}$, ω is the angular modulation frequency and L_i is the thickness of the layer i ($i = s, p$). In order to eliminate the instrumental factor V_0 , normalization procedure (a measurement with empty sensor) was applied [24]. After normalization, assuming thermally thick regime for both the detector and the sample ($\mu_i < L_i$), one can calculate the thermal diffusivity using the amplitude [Eq. (2)] and/or the phase [Eq. (3)] of the BPPE signal, respectively [3]:

$$\ln |V_n| = \ln \frac{2}{b_{sp} + 1} - L_s \left(\frac{\omega}{2\alpha_s} \right)^{1/2} \quad (2)$$

$$\Theta = \Theta_0 - L_s \left(\frac{\omega}{2\alpha_s} \right)^{1/2} \quad (3)$$

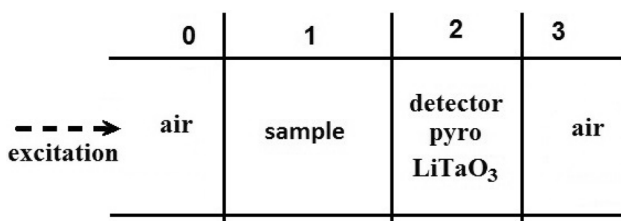


Fig. 1 Model of the four-layer system in the back PPE technique

In this paper, the thermal diffusivity was calculated using phase-lag method [26] from the slope a of the phase curve $\Theta = \Theta(f^{1/2})$, according to the following formula:

$$\alpha_s = \frac{L_s^2 \pi}{a^2} \quad (4)$$

4 Results and discussion

4.1 Surface study

Figure 2 presents AFM images of Zn_{0.9}Be_{0.05}Mn_{0.05}Se mixed crystals modified subsequently with various surface treatment procedures: grounding, polishing, etching and annealing, respectively, over the scan area $5 \times 5 \mu\text{m}^2$.

Short-range height variations (surface roughness, RMS) were expressed in terms of the root-mean-square standard deviation S_q . The ground sample (Fig. 2a) is found very rough (215 nm over $5 \times 5 \mu\text{m}^2$ scan area) although isotropic, the surface of which reveals neither second-order arrangement pattern nor directional alignment.

A polished specimen (Fig. 2b) exhibits finer and still homogeneous topography with the roughness 25.6 nm (over $10 \times 10 \mu\text{m}^2$ scan area), and a number of cavities 300 nm deep and 500 nm in size. On the nanoscopic level the surface topography appears to be generally flat, although rarely disturbed by the trenches 0.5 nm deep. The etched sample (Fig. 2c) is found even flatter than the previous one (the roughness less than 10 nm over area $5 \times 5 \mu\text{m}^2$), despite regular and parallel scratches (5–10 nm deep, 20–50 nm wide). Numerous grains of a foreign material smaller than 20 nm and approximated concentration $3 \times 10^{10} \text{ cm}^{-2}$ can be seen onto this surface.

Finally, the annealed sample (Fig. 2d) turns out the flattest (surface roughness smaller than 5 nm) with tiny, parallel scratches up to 1 nm in depth together with seed particles with the diameter of 200 nm, the height approaching 100 nm, and the concentration $1.5 \times 10^9 \text{ cm}^{-2}$. It is to notice that the scale of the z axis in Fig. 2d is cut-off at 15 nm, but this does not mean the maximum of the highest objects. The color scale was matched to the histogram of the altitude, so few of the high objects were truncated. The above observations can be concluded that the performed treatment procedures steadily improve the surface quality of the crystals.

Table 1 summarizes results of the characterization of the surface texture of the crystal under investigation using AFM images at two different scan lengths: 5 and $1 \mu\text{m}$ (see Fig. 3). As a rule, each treatment procedure leaves behind smoother surface except for the etching step, which reveals parallel trenches on the surface, and these contribute to higher surface roughness. On the other hand, the annealed sample appears to be the smoothest one throughout those

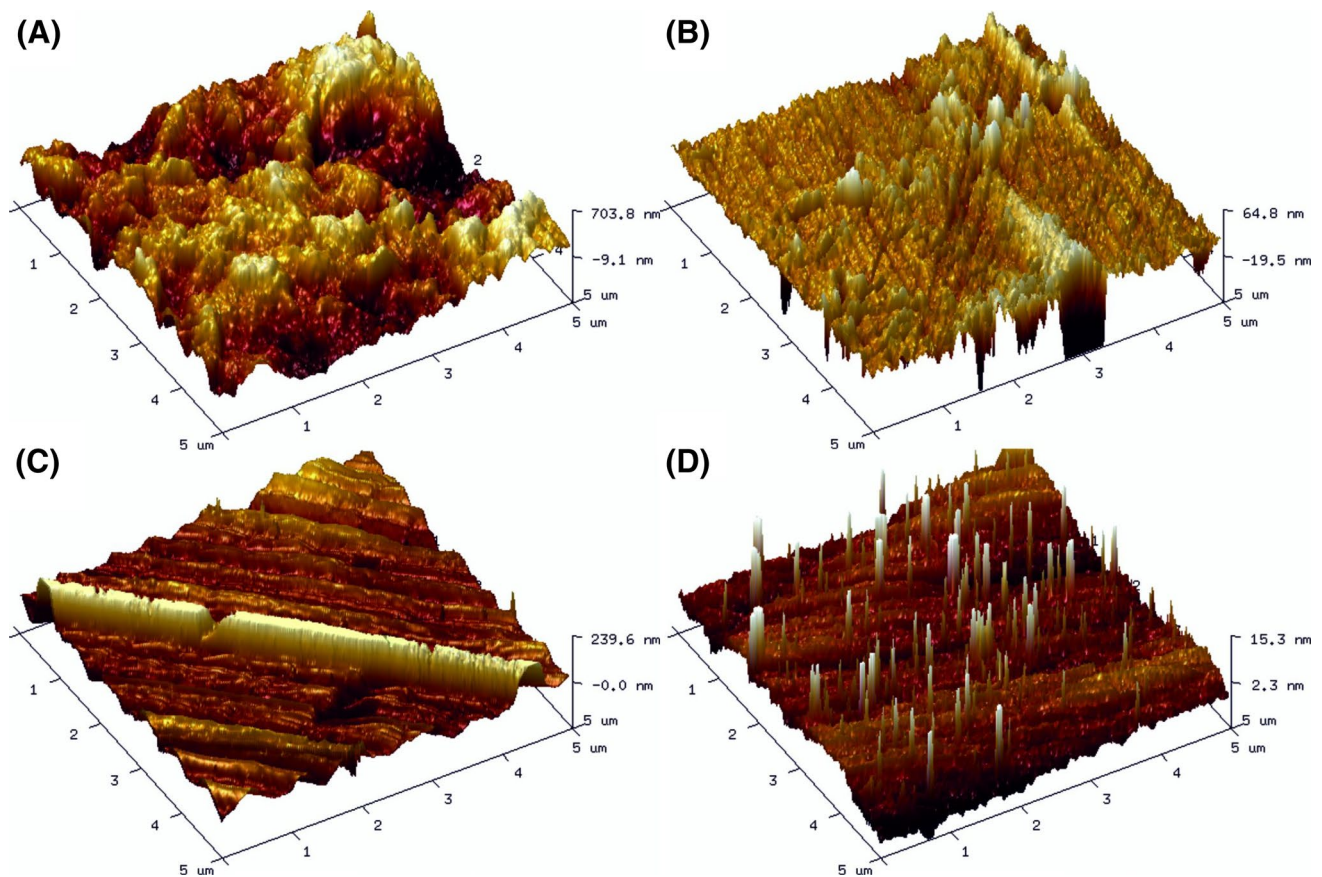


Fig. 2 AFM images of the $\text{Zn}_{0.9}\text{Be}_{0.05}\text{Mn}_{0.05}\text{Se}$ ground (a), polished (b), etched (c) and annealed (d) sample over the scan area $5 \times 5 \mu\text{m}^2$

Table 1 Surface texture characteristics of the investigated $\text{Zn}_{0.9}\text{Be}_{0.05}\text{Mn}_{0.05}\text{Se}$ crystal

| Sample | S_q [nm] 5 μm | S_q [nm] 1 μm | S_{al} [nm] 5 μm | S_{al} [nm] 1 μm | S_{tr} [nm] 5 μm | S_{tr} [nm] 1 μm |
|----------|----------------------------|----------------------------|-------------------------------|-------------------------------|-------------------------------|-------------------------------|
| Ground | 214 | 53.6 | 569 | 114 | 0.513 | 0.448 |
| Polished | 19.8 | 6.76 | 196 | 37 | 0.808 | 0.08 |
| Etched | 50.8 | 31.7 | 196 | 132 | 0.046 | 0.216 |
| Annealed | 3.75 | 1.64 | 137 | 48.5 | 0.254 | 0.124 |

under study approaching very low roughness less than 5 nm over the scan area $5 \times 5 \mu\text{m}^2$. The presence of trenches and other parallel ordered structures on the surface is reflected in the anisotropy ratio, which is found very low for highly anisotropic surfaces (e.g. etched sample) and goes close to unity for isotropic samples (e.g. polished surface). However, surface texture measures such as lateral decorrelation length S_{al} and anisotropy ratio S_{tr} shown in Table 1 appear to be largely scale-dependent, revealing the changes in the alignment and predominance of specific geometric patterns at various length scales. Because topographic factors might substantially affect the process of heat propagation through the PPE structure, more sophisticated, scale-invariant methods of surface texture characterization are necessary, which will be addressed in future works.

The surface of the $\text{Zn}_{0.79}\text{Be}_{0.05}\text{Mn}_{0.16}\text{Se}$ crystal with higher content of Mn ($x=0.16$) was investigated by means of both AFM (Fig. 4a) and MFM (Fig. 4b) methods, which brings parallel topographical and magnetic imaging. The sample presented in Fig. 4a exhibits flat, homogenous surface (the roughness equals to 6 nm) almost free of structural imperfections. The surface is relatively flat although a bundles of aligned trenches together with 20 nm dust particles (possibly abrasive residues) can be seen. Magnetic domains shown in Fig. 4b were measured with the lift height set at 50 nm. However, no magnetic domains became apparent even if the lift heights in the range 15–50 nm were used. This result agrees with high solubility of manganese observed for many II–VI Diluted Magnetic Semiconductors (DMS) [27]. DMS are materials with magnetic ions like Mn^{2+}

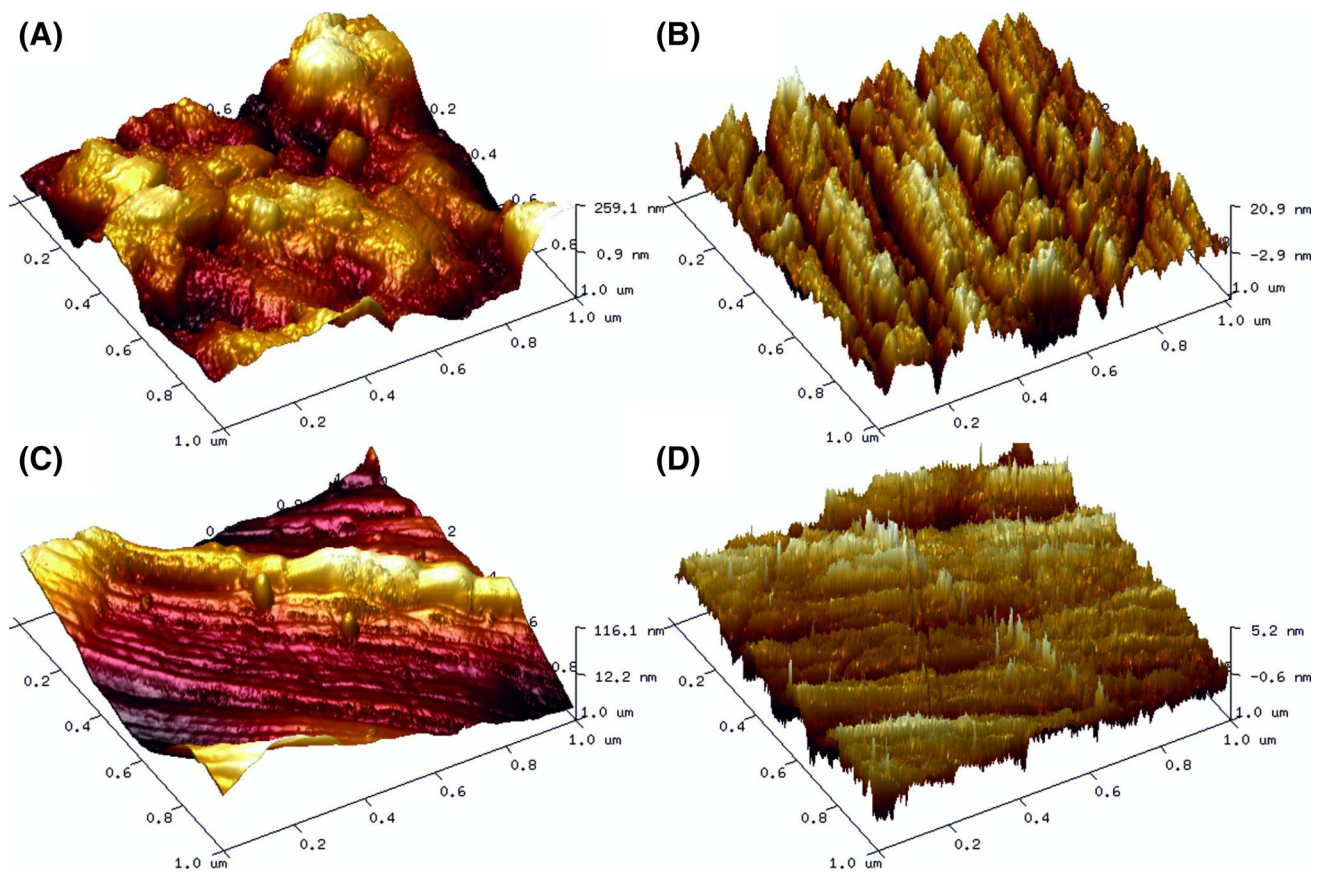


Fig. 3 AFM images of the $\text{Zn}_{0.9}\text{Be}_{0.05}\text{Mn}_{0.05}\text{Se}$ ground (a), polished (b), etched (c) and annealed (d) sample over the scan area $1 \times 1 \mu\text{m}^2$

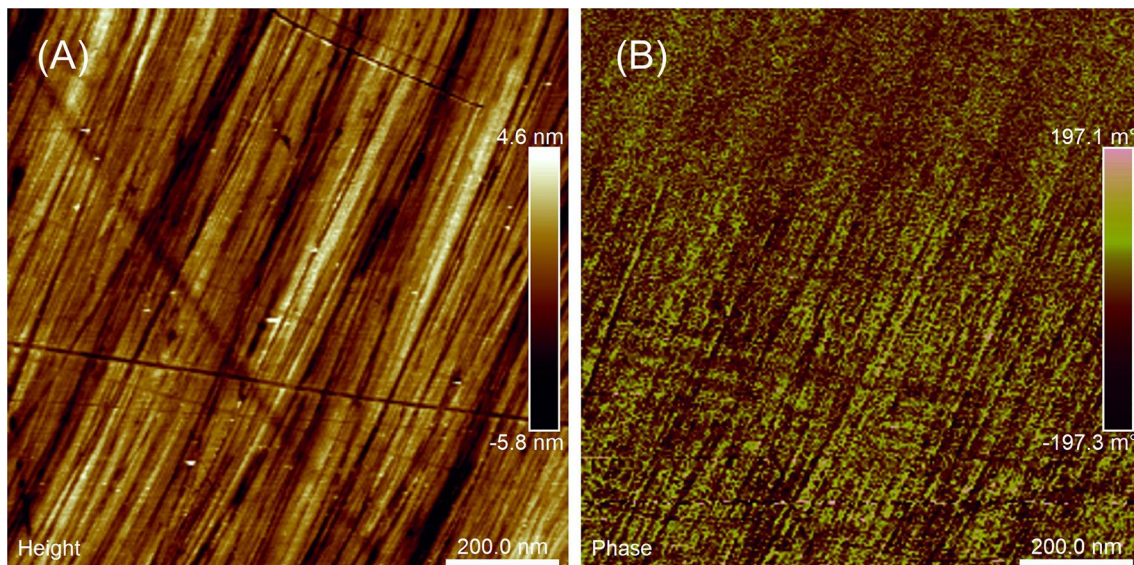


Fig. 4 AFM (a) and MFM (b) images of $\text{Zn}_{0.79}\text{Be}_{0.05}\text{Mn}_{0.16}\text{Se}$ crystal taken at lift height 50 nm

implemented into the crystal structure [28]. Potential magnetic domains could affect the propagation of the thermal wave throughout the sample, and hence the obtained value of the thermal diffusivity.

4.2 Photothermal study

Figure 5 presents the behavior of the phase of the PPE signal as a function of the square root of the modulation frequency for $\text{Zn}_{0.9}\text{Be}_{0.05}\text{Mn}_{0.05}\text{Se}$ crystals measured with PPE technique in the back detection configuration (BPPE) after each step of the surface treatment procedure. At lower frequencies (1–6 Hz), the curves exhibit slight deviation from the linearity due to the thermally thin regime of the sample or/and the sensor. Consequently, linear fits have been performed beyond that range (8–15 Hz), according to the requirements of the theory. For the fitting procedure, the least square method was applied. The determination coefficient R^2 , describing the quality of the fitting, was better than 0.9999 for all cases. Thermal diffusivities were calculated according to Eq. (4) from the slopes of the phase-sqrt(f) graphs.

In order to check the influence of the technological processes on the measured thermal diffusivity of the selected $\text{Zn}_{0.9}\text{Be}_{0.05}\text{Mn}_{0.05}\text{Se}$ sample, its value was measured after each step of surface treatment (see Table 2). It is worth to mention that in the case of the ground sample the damaged

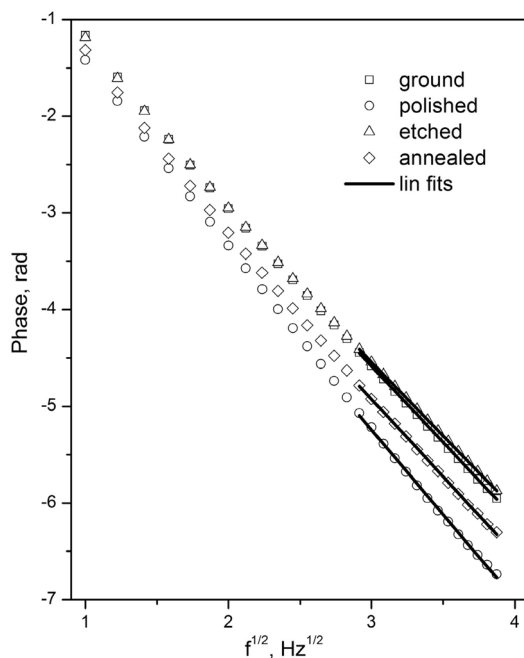


Fig. 5 The PPE phase characteristics the $\text{Zn}_{0.9}\text{Be}_{0.05}\text{Mn}_{0.05}\text{Se}$ crystal as a function of the square root of the modulation frequency (the points are experimental data and the lines are linear fits) for ground (squares), polished (circles), etched (triangles) and annealed sample (diamonds)

Table 2 Obtained parameters for the investigated $\text{Zn}_{0.9}\text{Be}_{0.05}\text{Mn}_{0.05}\text{Se}$ crystal for different surface preparation

| Sample | Thickness (mm) | Slope $s^{1/2}$ | Thermal diffusivity ($\text{m}^2 \text{s}^{-1}$) $\times 10^{-6}$ |
|----------|-----------------|-----------------|---|
| Ground | 1.46 ± 0.01 | -1.5763 | 2.695 ± 0.014 |
| Polished | 1.66 ± 0.01 | -1.7534 | 2.831 ± 0.015 |
| Etched | 1.44 ± 0.01 | -1.5210 | 2.837 ± 0.017 |
| Annealed | 1.62 ± 0.01 | -1.6025 | 3.221 ± 0.016 |

surface was faced to the sensor. Every sample was measured three times and the final result is given as average value with standard deviation as uncertainty. The thickness of the investigated samples was measured with a micrometer device (accuracy 10 μm). The BPPE is a contact method, in which a good thermal contact between the sample and the sensor is required. Therefore, the obtained value of the thermal diffusivity for the polished sample was also validated using non-contact infrared lock-in thermography (IRT) and it was taken from the already published work [29]. The values obtained for the thermal diffusivity of $\text{Zn}_{0.9}\text{Be}_{0.05}\text{Mn}_{0.05}\text{Se}$ crystal, by PPE and IRT were $(2.831 \pm 0.015) \times 10^{-6} \text{m}^2 \text{s}^{-1}$ and $(2.884 \pm 0.062) \times 10^{-6} \text{m}^2 \text{s}^{-1}$, respectively. The value of the thermal diffusivity obtained with PPE method is slightly smaller than measured by lock-in thermography, however, the difference is not large and lies within the error bars.

One can see in Table 2 the value of the measured thermal diffusivity of the ground sample is the lowest one; this fact can be connected with its highest roughness, which influences the thermal contact between the sample and the detector. The results obtained for polished and etched sample are practically the same; in this case also RMS values are similar. On the other hand, the annealed sample exhibits the highest thermal diffusivity value. This is not surprising since the first three treatment procedures influence only the surface of the samples, while the annealing process improves also the crystal structure. It is known that crystals produced by Bridgman-Stockbarger method exhibit high electrical resistance. The main source of this electrical resistance are cation vacancies, which become scattering centers for phonons. Annealing procedure in cation vapor reduces the concentration of these types of defects, and consequently the quality of the crystal as well as its thermal properties are getting better.

From the AFM data one can obtain surface development ratio (SDR) which can be calculated as a ratio of a real (triangulated) surface area taken from height samples to the projected area defined by the scan length (see Table 3). Note that the ratio is closely connected to surface height variability, and hence to the surface porosity.

According to the data, performed treatment procedure results in steadily decreasing development ratio, that is the

Table 3 Surface development ratio for Zn_{0.9}Be_{0.05}Mn_{0.05}Se crystals

| Sample | S_{SA}/S_{PA} [%] 5 μm | S_{SA}/S_{PA} [%] 1 μm |
|----------|-----------------------------|-----------------------------|
| Ground | 210 | 214 |
| Polished | 111 | 121 |
| Etched | 117 | 117 |
| Annealed | 101 | 104 |

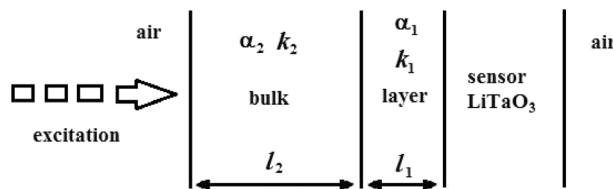


Fig. 7 Geometry for the two-layer system case

smoother surface for all cases. Note the trend that the surface development goes in the opposite direction compared to the thermal diffusivity.

It means that lesser surface development corresponds to better thermal diffusivity, which might be at least partly due to the imperfect sample/sensor interfacial contact. If so, it might be reasonable to extend the model at the interface including the fact that the layer stays in touch with the detector only locally. Alternatively, one might assume that the interface is made up of discontinuous layer material filled with the air. In such a picture thermal diffusivity of the layer is likely affected by that of the air, on the other hand, the thermal diffusivity of the material can be extrapolated from the non-linear (possibly exponential) thermal diffusivity vs. surface development plot (see Fig. 6). As such, the thermal diffusivity of the layer is the limit approached at 100% of the surface development ratio (flat surface).

The ground sample can be treated as two-layer system with different thermal parameters, where one layer is the

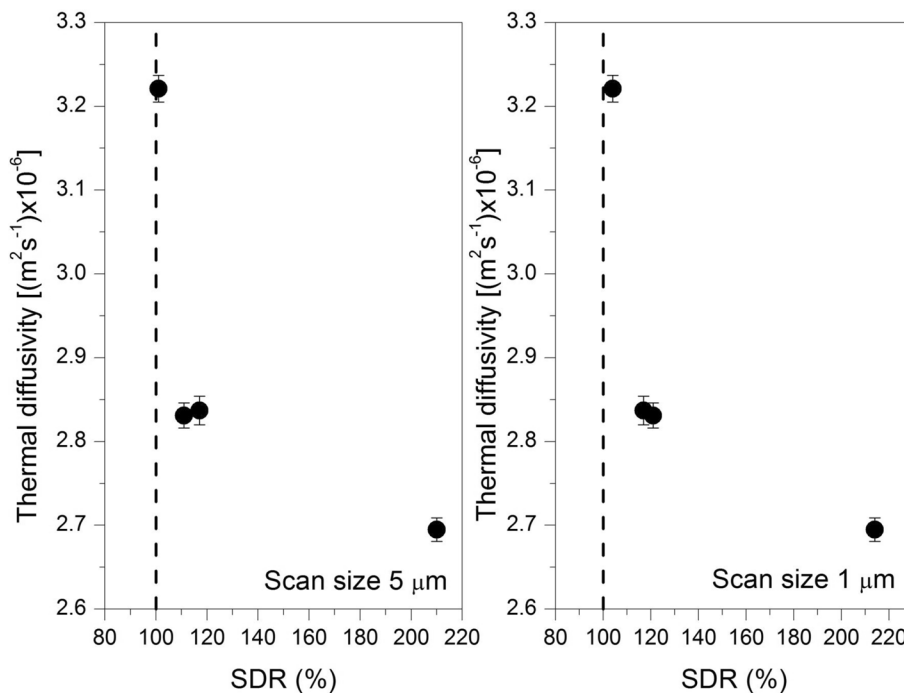
bulk material and the second one is the damaged layer (see Fig. 7).

Thanks to AFM investigations we can estimate the thickness of the second layer as 0.215 μm (RMS value). Now we will show that even so thin layer can significantly influence the obtained results. J.J. Alvarado-Gil et al. have shown that in the case of two-layer system the effective thermal diffusivity can be given by the following formula [30]:

$$\alpha_{\text{eff}} = \frac{1}{\frac{x^2}{\alpha_1} + \frac{(1-x)^2}{\alpha_2} + x(1-x)\left(\frac{\lambda}{\alpha_1} + \frac{1}{\lambda\alpha_2}\right)} \tag{5}$$

where: $x = l_1/l$ is the thickness ratio and $l = l_1 + l_2$, $\lambda = k_1/k_2$ and k_1 and k_2 are thermal conductivities of the damaged layer and bulk crystal, respectively, α_1 and α_2 are thermal diffusivities of the layers. This formula is a good approach for nearly stationary condition and our experiments were performed in the low-frequency regime.

Fig. 6 The thermal diffusivity as the function of the SDR values obtained for both scan size 5 μm and 1 μm presented on the left and right, respectively



We have assumed that measured thermal diffusivity in the case of the ground sample is the effective value α_{eff} for whole two-layer system $(2.695 \pm 0.014) \times 10^{-6} \text{ m}^2 \text{ s}^{-1}$. It is to mention that between the sample and the sensor there is still the thin coupling layer of the ethylene glycol, but in the first approximation we have neglected it here. On the other hand in the case of the bulk material we have taken the value obtained for polished sample $(2.831 \pm 0.015) \times 10^{-6} \text{ m}^2 \text{ s}^{-1}$. The real thermal conductivity of the polished sample was taken from [29] as $5.612 \pm 0.068 \text{ W m}^{-1} \text{ K}^{-1}$. Knowing the thicknesses of the layers only thermal conductivity and diffusivity of the damaged layer were to found. During calculations with Eq. (5) it has turned out that the effective thermal diffusivity depends much stronger on the conductivity ratio than on the diffusivity of the damaged layer. It is not surprising since the thermal conductivity strongly depends on the density of the medium (it is directly proportional) and the thermal diffusivity is inversely proportional. In other words, we expect here the thermal diffusivity of the damaged layer and the bulk material to be of the same order but having totally different thermal effusivities (two or even three orders in magnitude). In this case the two-layer formula in Eq. (5), provides much better results than the Tominaga and Ito equation [31] of the inverse square roots of the thermal diffusivity. Finally, the thermal conductivity ratio was found here as about 340, giving value of the thermal conductivity of the thin damaged layer $(0.0164 \text{ W m}^{-1} \text{ K}^{-1})$ smaller, however of the same order comparing to the air $(0.025 \text{ W m}^{-1} \text{ K}^{-1})$. This discrepancy can be explained by the fact of non-ideal thermal contact between the sample and the sensor and the presence of the coupling fluid within the system.

5 Conclusions

In this paper, the AFM imaging and the thermal diffusivity measurements of $\text{Zn}_{1-x-y}\text{Be}_x\text{Mn}_y\text{Se}$ crystals grown by high-pressure modified Bridgman-Stockbarger method and prepared with different surface treatment were carried out. The thermal diffusivity coefficients of the samples were obtained by the PPE method in the back detection configuration. Surface investigations performed with AFM technique showed a clear influence of the technological processes on the quality of the surface of investigated samples. MFM measurements confirmed the presumption of high solubility of manganese in the investigated materials. The average surface roughness of the crystals was found to decrease after each step of the technological process. Correlations between the RMS value as well as with the surface development ratio and the thermal diffusivity were found. Grounding, polishing and etching changed only the surface quality of the samples, while the annealing procedure improved the quality of the crystals. A higher thermal diffusivity value for the annealed crystal was

due to the reduced concentration of the cation vacancies. The quality of the contact surface affects in some extent the thermal diffusivity values measured by PPE technique. The ground sample was treated as two-layer system with different thermal parameters. The conductivity ratio between the bulk crystal and the damaged layer was about 340. One should keep in mind, that the obtained result is a combination of the thermal properties of the rough surface and the ethylene glycol which is in contact with it. The main problem was connected to the air being trapped within the contact, which significantly influences the obtained results leading to an effective value of thermal diffusivity and not to the absolute diffusivity of the bulk.

As a final remark, the different surface treatments influence the measured thermal diffusivity of the semiconductor crystals, the biggest variation being induced by the annealing process which improves the quality of the crystals.

Acknowledgements We are grateful to J.J. Alvarado-Gil for his valuable comments and time devoted for reading the manuscript.

Data availability The raw data required to reproduce these findings are available to download from [<https://data.mendeley.com/datasets/kpfxrwm3zv/draft?a=780aab3b-7b48-462a-80f3-1e319e40d958>]. The processed data required to reproduce these findings are available to download from [<https://data.mendeley.com/datasets/7k74fyf5wg/draft?a=f5781492-c1dd-4c54-9769-e77e10fa7425>].

Open Access This article is distributed under the terms of the Creative Commons Attribution 4.0 International License (<http://creativecommons.org/licenses/by/4.0/>), which permits unrestricted use, distribution, and reproduction in any medium, provided you give appropriate credit to the original author(s) and the source, provide a link to the Creative Commons license, and indicate if changes were made.

References

1. Ł. Chrobak, M. Malinski, J. Zakrzewski, *Thermochim. Acta* **606**, 84 (2015)
2. D. Korte, E. Pavlica, G. Bratina, F. Mladen, *Int. J. Thermophys.* **35**, 1990 (2014)
3. D. Dadarlat, *Laser Phys.* **19**, 1330 (2009)
4. D. Dadarlat, M. Streza, O. Onija, C. Prejmerean, L. Silaghi-Dumitrescu, N. Cobirzan, K. Strzałkowski, *J. Therm. Anal. Calorim.* **119**, 301 (2015)
5. A. Salazar, *Rev. Sci. Instrum.* **74**, 825 (2003)
6. A. Salazar, Oleaga, *Rev. Sci. Instrum.* **83**, 014903 (2012)
7. M. Marinelli, F. Mercuri, U. Zammit, R. Pizzoferrato, *Appl. Phys. A* **52**, 115 (1991)
8. K. Strzałkowski, D. Dadarlat, M. Streza, F. Firszt, *Thermochim. Acta* **614**, 232 (2015)
9. J.S. Antoniow, M. Chirtoc, R. Drevet, C. Jensen, H. Benhayoune, *Int. J. Thermophys.* **33**, 1960 (2012)
10. H.G. Walter, *Appl. Surf. Sci.* **193**, 156 (2002)
11. M. Chirtoc, in *Thermal wave physics and related photothermal techniques: basic principles and recent developments*, ed. by E. Martin (Transworld Research Network, Trivandrum, 2009), pp. 29–63. (chap. 2)

12. B. Bein, S. Krueger, J. Pelzl, *Can. J. Phys.* **64**, 1208 (1986)
13. J.A. Garcia, A. Mandelis, B. Farahbakhsh, C. Lebowitz, I. Harris, *Int. J. Thermophys.* **20**, 1587 (1999)
14. H.G. Walther, M.C. Larciprete, P. Mayr, S. Paoloni, B. Schmitz, *Anal. Sci.* **17**, 428 (2001)
15. J.A. Garcia, L. Nicolaidis, P. Park, A. Mandelis, B. Farahbakhsh, *Anal. Sci.* **17**, 89 (2001)
16. L. Nicolaidis, A. Mandelis, *J. Appl. Phys.* **90**, 1255 (2001)
17. K. Moojoong, K. Gwantaek, Y. Jaisuk, K. Dong-Kwon, K. Hyun-jung, *Thermochim. Acta.* **661**, 7 (2018)
18. M. Maliński, M. Pawlak, Ł. Chrobak, S. Pal, A. Ludwig, *Appl. Phys. A* **118**, 1009 (2015)
19. M. Pawlak, S. Pal, A. Ludwig, A.D. Wieck, *J. Appl. Phys.* **122**, 135109 (2017)
20. F. Firszt, S. Łęgowski, H. Męczyńska, J. Szatkowski, W. Paszkowicz, K. Godwod, *J. Cryst. Growth* **184/185**, 35 (1998)
21. F. Firszt, K. Strzałkowski, J. Zakrzewski, S. Łęgowski, H. Męczyńska, M. Malinski, D.O. Dumcenco, C.T. Huang, Y.S. Huang, *Phys. Status Solidi B* **247**, 1402 (2010)
22. A.A. Wronkowska, K. Bejtka, H. Arwin, A. Wronkowski, F. Firszt, S. Łęgowski, H. Męczyńska, A. Marasek, *Thin Solid Films* **455–456**, 256 (2004)
23. R.B. Bylisma, W.M. Becker, J. Kossut, U. Debska, D. Yoder-Short, *Phys. Rev.* **33**, 8207 (1986)
24. A. Mandelis, M.M. Zver, *J. Appl. Phys.* **57**, 4421 (1985)
25. M. Chirtoc, G. Mihailescu, *Phys. Rev. B* **40**, 9606 (1989)
26. Ł. Chrobak, M. Malinski, *Arch. Acoust.* **34**, 727 (2009)
27. G. Theurich, N.A. Hill, *Phys. Rev. B* **66**, 115208 (2002)
28. S.J. Pearton, C.R. Abernathy, D.P. Norton, A.F. Hebard, Y.D. Park, L.A. Boatner, J.D. Budai, *Mat. Sci. Eng. R* **40**, 137 (2003)
29. K. Strzałkowski, D. Dadarlat, M. Streza, J. Zakrzewski, *Appl. Phys. A* **119**, 1165 (2015)
30. J.J. Alvarado-Gil, O. Zelaya-Angel, F. Sanchez-Sinencio, H. Vargast, J.L. Lucio, *Vacuum* **46**, 883 (1995)
31. T. Tominaga, A. Ito, *Space. Appl. Phys.* **27**, 2392 (1988)

Publisher's Note Springer Nature remains neutral with regard to jurisdictional claims in published maps and institutional affiliations.